(Received 1 August 2025, Accepted 22 September 2025, Scheduled 4 October 2025)

Low Profile Metasurfaces Based Stacked Slotted Microstrip Antenna in a Ring for 5G Applications

Vijaypal Yadav[1], Meenakshi Awasthi[1], and Rajiv Kumar Gupta[2, *]

[1] *Department of Electrical, Electronics and Communication Engineering, Galgotia University, India*
[2] *Department of Electronics and Communication Engineering, Ramrao Adik Institute of Technology D Y Patil Deemed to be University, Navi-Mumbai, India*

ABSTRACT: This paper proposes a stacked slotted microstrip antenna (MSA) using multiple metasurfaces which offers high gain and stable radiation patterns for 5G applications. A metal-plated suspended MSA (SMSA) in air is designed to enhance gain and bandwidth (BW). However, impedance becomes inductive, and the cross-polarization level (CPL) increases with the increase in probe feed length. To decrease the inductive impedance and increase the capacitance, a slot in the SMSA is etched. A parasitic patch with metasurfaces on a superstrate is placed above the slotted SMSA, and a rectangular ring around the slotted MSA is designed to increase the inductance. To compensate it, substrate height is decreased. The decrease in probe feed length/substrate height decreases the CPL. Parasitic patch, rectangular ring around slotted SMSA, and metasurfaces electromagnetically couple with SMSA and enhance the BW of the antenna. The low-profile ($0.979\lambda \times 1.03\lambda \times 0.064\lambda$, λ — wavelength in free-space at 3.3 GHz) antenna offers the peak gain of 9.8 dBi and antenna efficiency $> 80\%$; SLL and CPL are < -22 dB; and the gain variation is < 0.5 dB over the 3.3–3.6 GHz frequency band for 5G application. The substrate height of the proposed novel structure is 2.5 times less than SMSA, and it offers an improvement of 8.1 dB in CPL as compared to SMSA.

1. INTRODUCTION

High data rate with low latency and seamless connectivity offered by 5G technology has affected every field. It has not only boosted wireless communication but also provided comfort and upgradation to every field like education, medicine, agriculture, entertainment, internet of things (IOT), home automation, automobile, robotics, textile, and interior decoration industry through augmented and virtual reality. The young generation is familiar with the advancement and advantages of wireless systems and thus, extensively uses 5G wireless systems. However, radio frequency radiations are reported to be biologically harmful and cause health hazards to human beings, animals, and plants. Thus, wireless systems and especially antennas need to be designed properly so as to avoid undesirable radiation in unintended directions, which may interfere with other devices.

Effective power in the desired direction increases with increase in the gain of an antenna; therefore, high-gain antennas are fed with low power. However, a high-gain antenna must have low sidelobe level (SLL) and CPL to mitigate interference and health hazards. MSA designed on a low permittivity and thick dielectric substrate offers higher gain but has larger dimensions [1]. Radiating/non-radiating edge-coupled planar and stacked multi-resonator patches offer wide BW; however, radiation patterns vary over wide BW [2–4]. A stack of circular patches over a metallic elliptical patch is designed. The structure offers 12.1 dBi gain and 55.7% BW [2]. A two-cavity stacked antenna designed as a multi-resonators provides 12.5 dBi gain in [3]. A circularly polarized (CP) square slot antenna is truncated at the corner and loaded with a rectangular ring to achieve 39% 3-dB axial ratio bandwidth (ARBW) [4]. A stacked antenna using triangular patches is designed to provide 10.8 dBi gain with high SLL of -13.6 dB and low front-to-back lobe ratio (FBR) of 15.8 dB [5]. A dual-band antenna consisting of a stack of two patches with E-shape and U-shape slots is designed [6]. However, these antenna structures have high SLL or CPL. Suspended MSAs (SMSAs) are designed for higher gain and BW, but in SMSAs, CPL increases with the increase in probe feed length. Wide BW systems also suffer from poor signal-to-noise ratio (SNR).

Metasurfaces (MSs) have attracted the attention of researchers as these surfaces control the properties of electromagnetic fields viz., polarization, phase, and magnitude of fields and therefore, can be designed to achieve desirable performance of an antenna [7, 8]. MS is an array of unit cells whose dimensions and periodicity are less than one-tenth of the operating wavelength. Further, nonuniform, defective, and anisotropic MSs have been explored by researchers. Antennas using an anisotropic elliptical MS in [9] and a nonuniform MS [10] are designed to enhance the ARBW. Reactive impedance surface (RIS) and frequency selective surface (FSS) are employed to design a wide-band CP antenna in [11]. A CP antenna using two arrangements of arrays of truncated corner patches is designed to achieve 75% 3-dB ARBW [12]. MS is modified to enhance gain and BW in [13]. Aperture efficiency is improved by designing a non-zero-index

* Corresponding author: Rajiv Kumar Gupta (rajivmind@gmail.com).

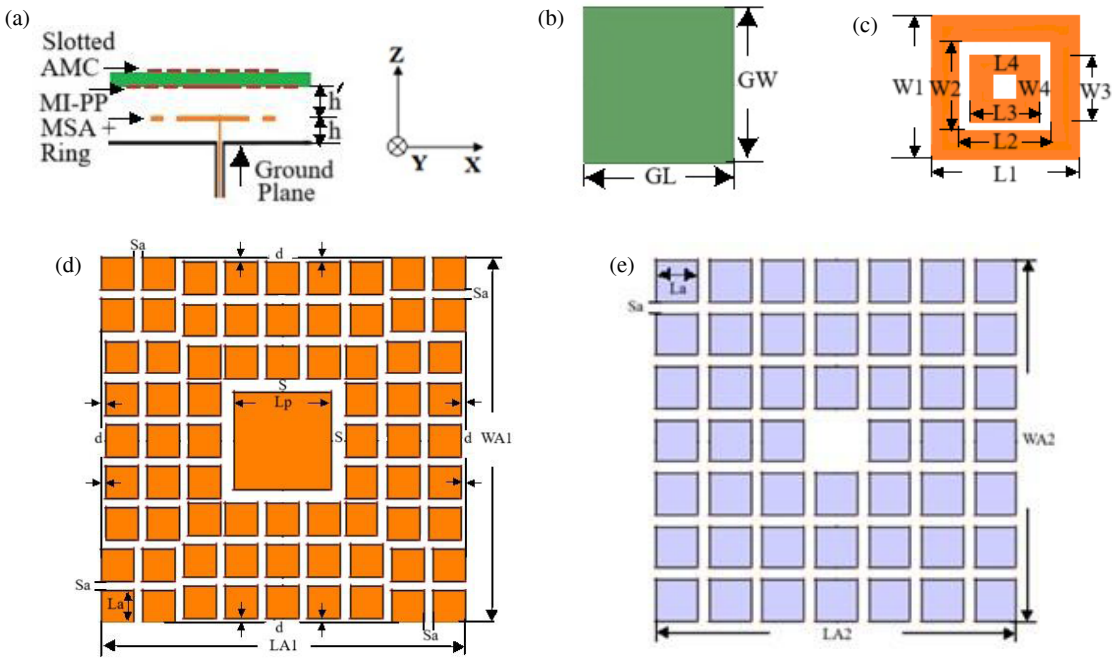

FIGURE 1. Geometry of proposed antenna ($h = 1.8$, $h' = 2.4$, $GL = 89$, $GW = 94$, $L1 = 74$, $L2 = 46$, $L3 = 34.4$, $L4 = 10.4$, $W1 = 74$, $W2 = 46.5$, $W3 = 36$, $W4 = 12$, $LA1 = WA1 = 79$, $Lp = 21$, $S = 3$, $La = 7$, $Sa = 2$, $d = 1$, $LA2 = WA2 = 61$. All dimensions are in mm. (Figures are not to scale). (a) Side view. (b) Ground plane. (c) Slotted MSA in a ring. (d) Metamaterial-inspired parasitic patch. (e) slotted AMC surface.

near-zero index (NZI) MS lens in [14]. Multiple uniform MSs are designed [15] while a slotted artificial magnetic conducting (AMC) surface and reactive impedance surface (RIS) are employed [16] to enhance the BW of the MSA array. A metamaterial loaded triple-band antenna has been reported in [17]. The stacked configurations employing RIS, AMC, metamaterial-inspired MSA, and a parasitic patch are designed [18, 19]. Antenna structures offer wide bandwidth and improved radiation characteristics with low CPL and SLL. However, these structures have low gain. A comprehensive study on applications of MSs is discussed and analyzed in [20, 21]. An MS-loaded antenna is employed for imaging and synthetic aperture radar applications in [22].

A truncated square patch surrounded by metasurface cells is placed in a Fabry-Perot Cavity (FPC) having a phase gradient partially reflecting metasurface (PRMS) to achieve 9.8% 3-dB ARBW. Beam deflection is obtained by rotating PRMS [23]. A frequency- and polarization-reconfigurable planar slot antenna is designed using a metasurface and a reflector. The antenna offers a peak gain of 16.5 dBi and fractional bandwidth of 33.3% [24]. The ground plane, partially reflecting surface, and MS are modified in high-gain FPC antennas [25, 26]. A low-profile MS-based stacked antenna is designed to feed an FPC antenna. The antenna offers 16.5 dBi peak gain with < -20 dB CPL [27]. However, these antennas have large dimensions and high profile.

In this article, a novel high-gain metal-plated antenna using multiple metasurfaces is proposed. The structure consists of a metal-plated slotted SMSA surrounded by a metallic ring, a metamaterial-inspired parasitic patch (MI-PP), and a slotted AMC on a superstrate. The low-cost simple to design and fabricate $0.979\lambda_0 \times 1.03\lambda_0 \times 0.064\lambda_0$ structure offers a peak gain of 9.8 dBi, antenna efficiency $> 80\%$, SLL and CPL < -22 dB, and the gain variation is < 0.5 dB over the 3.3–3.6 GHz frequency band for 5G application. The substrate height of the proposed novel structure is 2.5 times less than SMSA, and it offers an improvement of 8.1 dB in CPL as compared to SMSA. The paper is organized as follows. Antenna geometry with design theory is discussed in Section 2 while Section 3 deals with the simulation results and analysis. Fabrication and measurement results are presented in Section 4 followed by a conclusion in Section 5.

2. ANTENNA GEOMETRY AND DESIGN THEORY

Gain and BW of MSA can be increased by using a low dielectric constant substrate and increasing the substrate height. Since air has the lowest dielectric constant and negligible dielectric loss, a metal-plated SMSA (MPSMSA) suspended in air offers higher gain. However, due to radiation from the probe feed, CPL increases with the increase in substrate height. Antenna impedance also becomes inductive and causes impedance mismatch when the substrate height is increased beyond a limit, resulting in a decrease in impedance BW. Thus, there is a trade-off among substrate height, BW, and CPL. Different techniques have been reported to increase BW, but little work has been carried out to improve CPL. A novel stacked slotted metal-plated SMSA in a ring is designed using metasurfaces (Fig. 1) to achieve 8.1 dB improvement in CPL by decreasing the substrate height 2.5 times as compared to SMSA. The antenna also of-

fers comparable gain and broader bandwidth than metal-plated SMSA.

A slot in a metal-plated SMSA increases the inductance due to the increase in effective current density on the conducting metal surface (Fig. 1(c)). Metasurfaces are designed on a superstrate and placed above the slotted SMSA to increase the inductive impedance of the antenna. Inductive impedance is further increased by designing a MI-PP — a parasitic patch surrounded by an array of square patches (side dimension and spacing between the square patches $< 0.1\lambda$) on one side and a slotted AMC on the other side of a 1.6 mm FR4 ($\tan\delta = 0.02$, $\varepsilon_r = 4.4$) superstrate (Fig. 1(d) and Fig. 1(e)). The slotted SMSA is also surrounded by a rectangular ring to increase inductance (Fig. 1(c)). The increase in inductance is compensated by decreasing the substrate height 'h', which results in the decrease in CPL.

The side view of the proposed multilayer antenna, along with the top view of the different layers — metal-plated ground plane, slotted MSA in a ring, metamaterial-inspired parasitic patch, and slotted AMC — is shown in Fig. 1. Different layers of the stacked antenna are designed to resonate at nearby frequencies to electromagnetically couple and enhance the BW of the antenna. The square patches of MI-PP and slotted AMC are equivalent to inductors, and the spacing between patches acts as a capacitor. In MI-PP, the spacing between patches is varied to tune and achieve the desired BW. Slotted MSA dimensions, ring dimensions, and spacing between ring and slotted SMSA, PP dimensions, and slot dimensions, as well as the height of SMSA and spacing between SMSA and superstrate (h'), are optimized to obtain the desired BW of 3.3–3.6 GHz and CPL < -22 dB.

Square ring around slotted SMSA is equivalent to L-C network in which the conducting surface acts as an inductor L_1, while the spacing between the ring and SMSA acts as a capacitor C_1. Slotted SMSA acts as an L_2-C_2 network. The probe feed is a shortened transmission line and acts as an inductor 'L', while the spacing between SMSA and ground plane acts as a capacitor 'C'. A conducting parasitic patch in slotted AMC or MI-PP is equivalent to inductor L_3, while the spacing between patches is capacitor C_3. The conducting patches on different layers form inductance, and the spacing between layers acts as a capacitor. The equivalent circuit of a stacked slotted SMSA with a ring and metasurfaces is shown in Fig. 2 [16]. The electromagnetic coupling between the ring and slotted SMSA, and SMSA and MI-PP with slotted AMC forms mutual inductance and capacitance L_{M1} and C_{M1}, and L_{M2} and C_{M2}, respectively. Inductance is increased by placing a ring around slotted SMSA, PP, and square patches around PP and AMC, and then the SMSA height is decreased not only to increase capacitance but to decrease CPL and obtain a low-profile structure. Dimensions of SMSA and slot, ring, PP, slot in AMC, SMSA height, and spacing between SMSA and superstrate layer are optimized so that the antenna operates over 3.3–3.6 GHz.

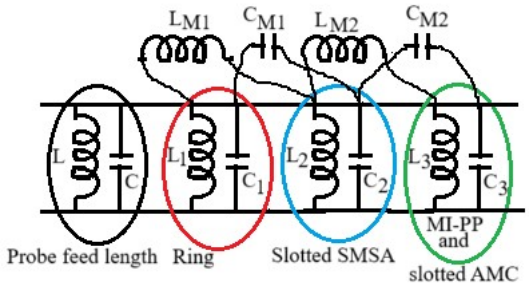

FIGURE 2. Equivalent circuit of a stacked slotted SMSA in a ring with meta-surfaces.

3. SIMULATION RESULTS AND ANALYSIS

3.1. Suspended MSA (SMSA), Metal-Plated SMSA, and Metal-Plated Slotted SMSA

Initially, a rectangular MSA of 19.8 mm × 24.3 mm is designed on a 1.59 mm-thick FR4 substrate. The ground plane dimensions are 50 mm × 55 mm. The antenna offers the peak gain of 4.0 dBi and $S_{11} \leq -10$ dB over 3.4–3.51 GHz. The dimensions of the antenna are calculated using standard equations [1]. All structures are simulated using IE3D 15.0 version software. To enhance the BW and gain of the antenna, a suspended MSA (SMSA) on an FR4 substrate, as shown in Fig. 3(a), is designed. A rectangular MSA of 30 mm × 35 mm is designed on an FR4 substrate and suspended in air at 3.5 mm from 80 mm × 85 mm ground plane. The SMSA offers the peak gain of 8.1 dBi, CPL < -13.3 dB, and $S_{11} \leq -10$ dB over 3.3–3.56 GHz.

A 0.5 mm thick copper metal-plated suspended MSA (MPSMSA) is designed and suspended from a metal-plated ground plane at 5 mm (Fig. 3(b)). Since air is used as a dielectric, the antenna offers high efficiency and polarization purity due to the absence of surface waves; however, the antenna needs to be mechanically realized using LASER metal cutting technology. The antenna also has large dimensions due to low dielectric constant. The 38.8 mm × 45 mm MSA is placed at 5 mm from 93 mm × 98 mm ground plane. The antenna offers the peak gain of 10.1 dBi, CPL < -13.9 dB, and $S_{11} \leq -10$ dB over 3.28–3.53 GHz. A metal-plated slotted SMSA (MPSSMSA) is designed (Fig. 3(c)) as a slot at the center increases the effective surface current density on the conducting metal surface and increases the inductance; therefore, the air gap 'h' is decreased to increase the capacitance and improve bandwidth (BW). 37.6 mm × 45 mm slotted SMSA has a 10 mm × 12 mm slot at the center and is placed at 4.5 mm from 93 mm × 98 mm ground plane. The antenna offers the peak gain of 10.1 dBi, CPL < -14.4 dB, and $S_{11} \leq -10$ dB over 3.3–3.53 GHz. The side and top views of these antenna structures are shown in Fig. 3. The impedance variation and return loss are depicted in Fig. 4, while gain and antenna efficiency are shown in Fig. 5. The radiation patterns at 3.45 GHz are shown in Fig. 6. Scalar and vector surface current distributions over the patch and ground plane are shown in Fig. 7. In SMSA, there is considerable surface current on the ground plane as compared to MPSMSA and MPSSMSA. It results in more losses and less fringing fields, and therefore less gain. In SMSA, especially near the feed point, the magnitude of surface current in the orthogonal direction is greater than MPSMSA and MPSSMSA, resulting

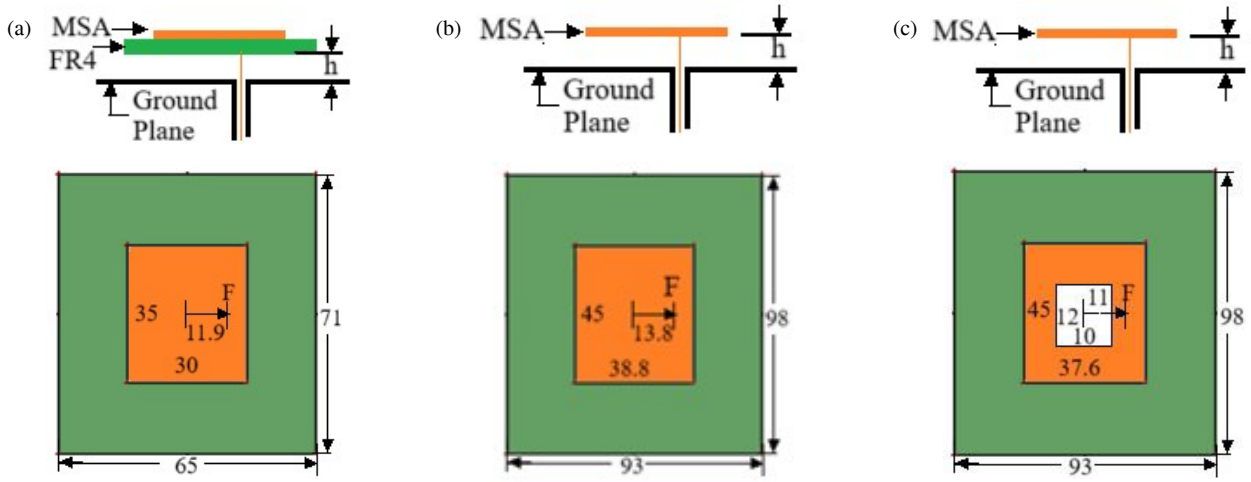

FIGURE 3. Side and top views of (a) SMSA ($h = 3.5$), (b) MPSMSA ($h = 5.0$), (c) MPSSMSA ($h = 4.5$). All dimensions are in mm only. F represents the feed point along the x-axis.

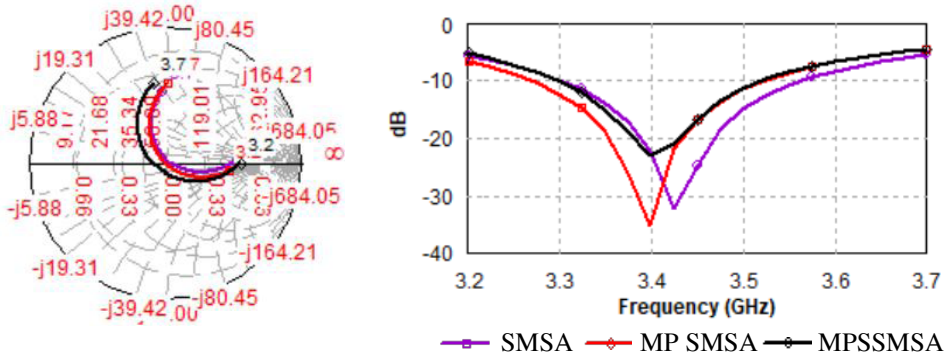

FIGURE 4. Impedance variation and return loss.

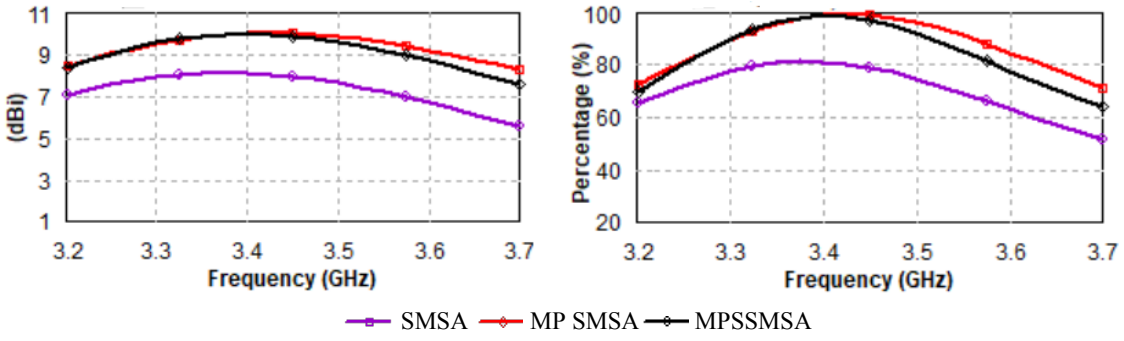

FIGURE 5. Gain and antenna efficiency.

in a higher CPL than MPSMSA and MPSSMSA. The surface current in the orthogonal direction is in the opposite direction in MPSSMSA, resulting in lower CPL than SMSA.

3.2. MPSSMSA with Uniform AMC, Slotted AMC, and Two Slotted AMC Surfaces

The metal-plated SMSA does not cover the desired BW from 3.3 to 3.6 GHz for 5G applications and also has high SLL and CPL. Therefore, to decrease SLL and CPL and to improve BW, a uniform artificial magnetic conductor (AMC) layer is fabricated on an FR4 substrate and placed above the MPSSMSA (Fig. 8(a)). The dimension and periodicity of the array of square patches of metamaterial surface, viz., AMC is $< 0.1\lambda_0$. A 9×9 array of 7 mm square patches with a periodicity of 9 mm forms the AMC layer. A slotted AMC (SAMC-1) is incorporated in Fig. 8(b) by removing a 5×5 array of square patches from the uniform AMC. In Fig. 8(c), another slotted AMC (SAMC-2) is fabricated on the other side of the FR4 superstrate.

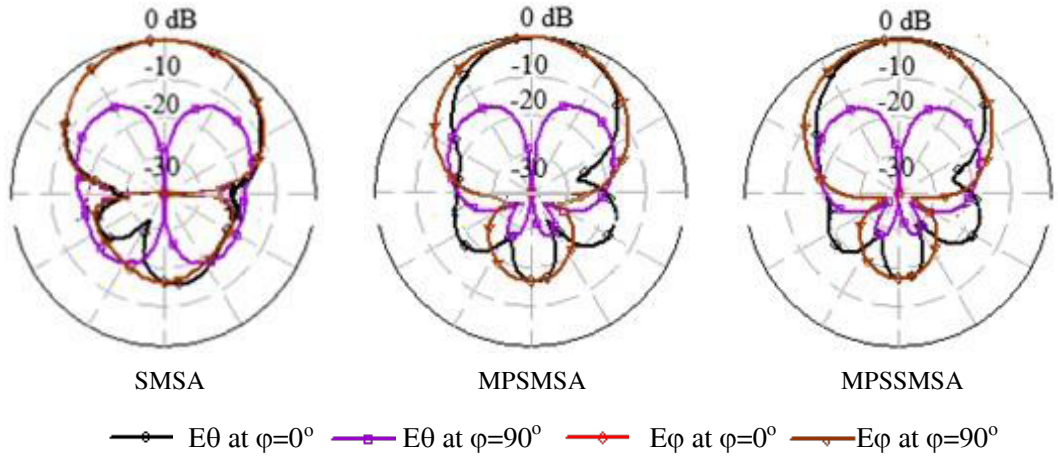

FIGURE 6. Radiation pattern is at 3.45 GHz (Eφ at $\varphi = 0^\circ < -40$ dB, and therefore, it is not visible in the radiation plots).

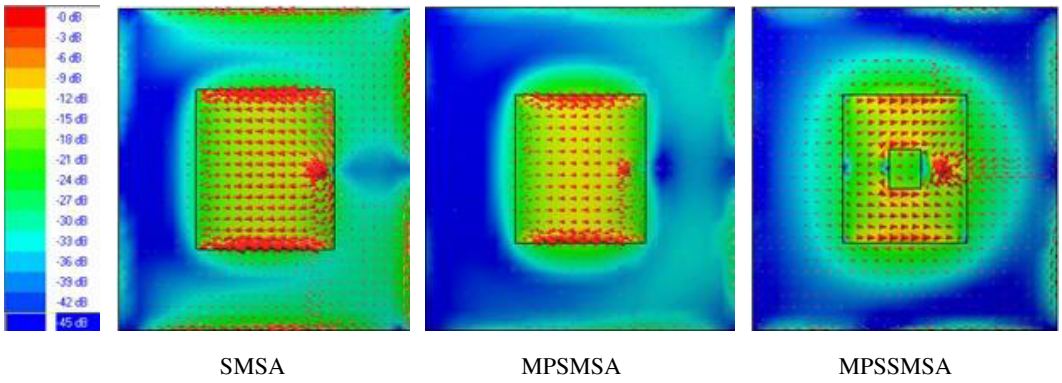

FIGURE 7. Scalar and vector surface current distributions.

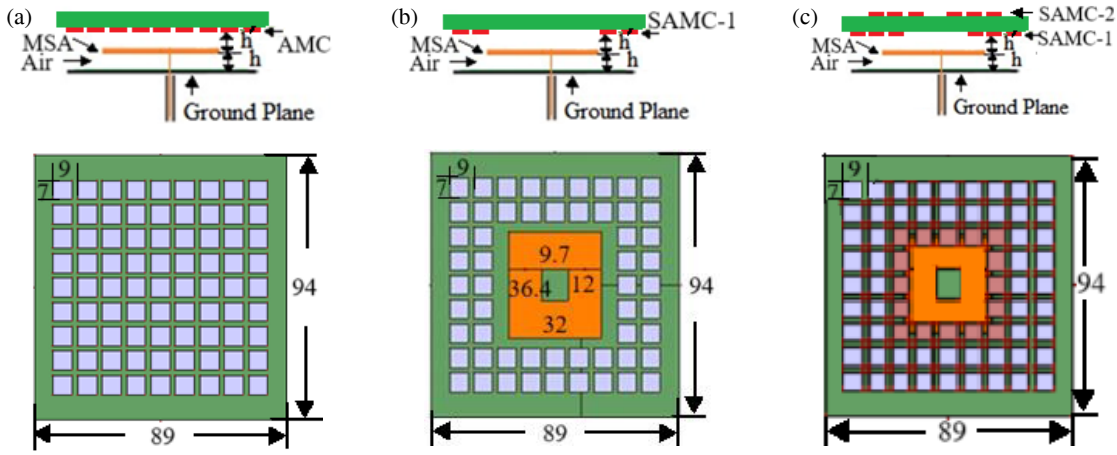

FIGURE 8. Side and top views of MPSSMSA with (a) uniform AMC ($h = 4$, $h' = 2$), (b) slotted AMC ($h = 4$, $h' = 2$), (c) two slotted AMC ($h = 4$, $h' = 2$).

The AMC layer increases the inductive impedance; therefore, the structure is optimized, and the feed point is shifted to the right to improve the impedance matching. $S_{11} < -10$ dB is obtained over 3.28–3.63 GHz. AMC enhances the impedance BW as the AMC layer electromagnetically couples with MPSSMSA. At fixed substrate height, $h = 4.5$ mm, impedance variation and return loss of MPSSMSA, MPSSMSA with a uniform AMC layer (MPSSMSA-AMC) and optimized structure of MPSSMSA with uniform AMC layer (MPSSMSA-AMC-opt) are shown in Fig. 9.

Alternatively, to compensate the inductive impedance, the substrate height 'h' is decreased to 4.0 mm to increase the capacitance. CPL decreases with decrease in 'h'. CPL < -14.8 dB is obtained, but it is still high. A slot in AMC de-

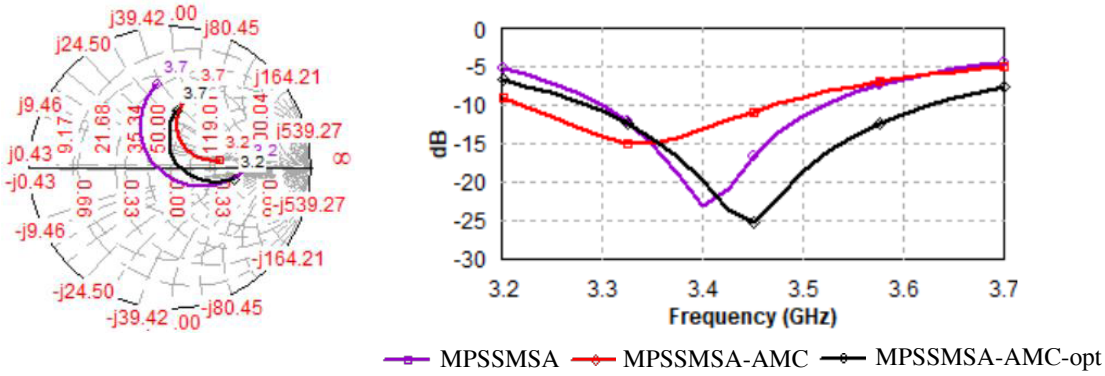

FIGURE 9. Impedance variation and return loss.

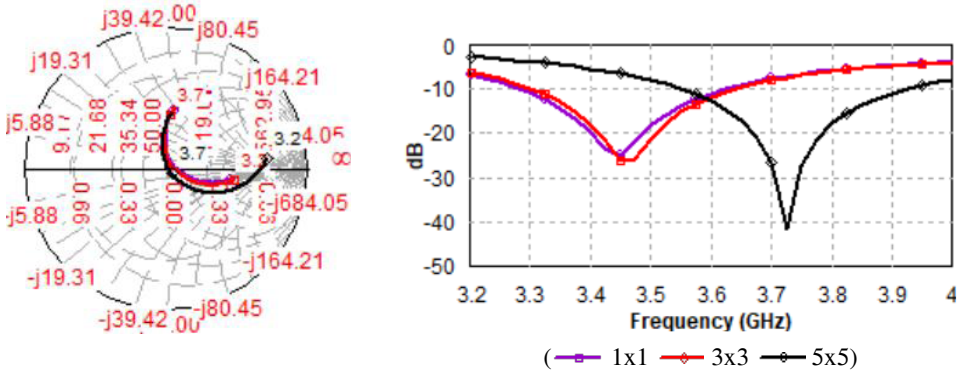

FIGURE 10. Impedance variation and return loss for different slot sizes in MPSSMSA with single SAMC.

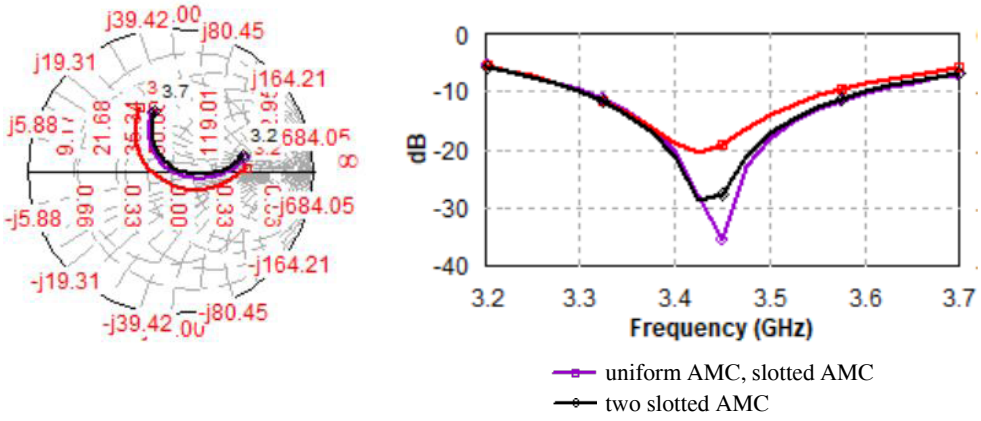

FIGURE 11. Impedance variation and return loss of MPSSMSA.

creases the inductance due to conducting metal patches and also introduces a capacitance. Slot dimensions in AMC affect the impedance BW of the antenna. By varying the size of the slot, we can vary the reactive impedance and therefore, BW of the structure. The effect of slot size on impedance variation and S_{11}, shown in Fig. 10, is analyzed. The resonant frequency increases with an increase in slot size in AMC. The AMC increases the inductive impedance of the structure, while a slot in the AMC surface and a decrease in substrate height increase the capacitive impedance. The MPSSMSA structures with uniform AMC, single SAMC, and two SAMC are optimized. MPSSMSA with uniform AMC and two SAMCs offers the same BW, but CPL < -15.2 dB and -15.4 dB are obtained in MPSSMSA with single and two SAMCs, respectively. Impedance variation and return loss of MPSSMSA with uniform AMC, single SAMC, and two SAMCs are shown in Fig. 11. The slot size in AMC affects the impedance BW and CPL. Therefore, an attempt is made to reduce the substrate height by optimising a two-SAMC structure with different slot sizes in two AMCs.

MPSSMSA with two slotted AMCs is designed for different 'h'. The slots of both AMCs, spacing between substrate

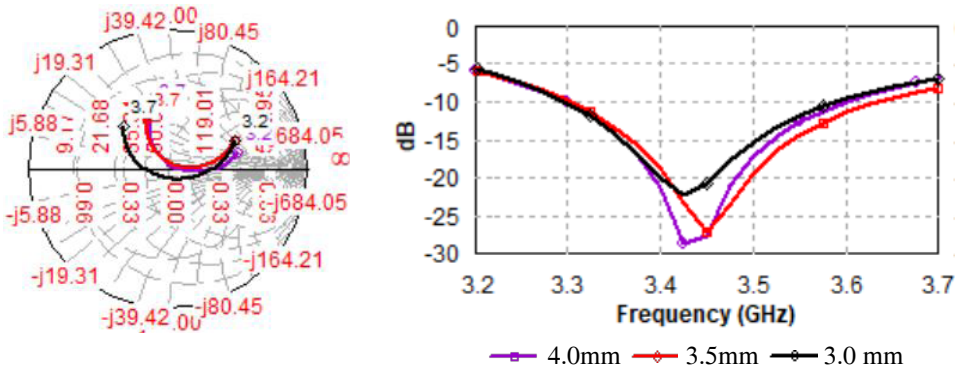

FIGURE 12. Impedance variation and return loss of MPSSMSA with two slotted AMCs at different h.

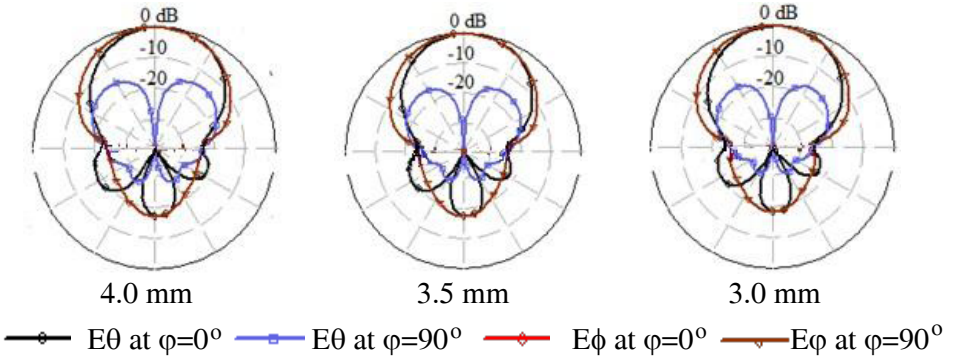

FIGURE 13. Radiation pattern at 3.45 GHz.

and superstrate, and MSA dimensions are optimized to obtain $S_{11} < -10$ dB over 3.3–3.6 GHz. (i) At $h = 4.0$ mm, $h' = 2.0$ mm, 9×9 array AMC-1 has a slot of a 5×5 array of square patches while 5×5 array of AMC-2 has a slot of a 3×3 array of square patches. (ii) At $h = 3.5$ mm, $h' = 2.5$ mm, 9×9 array AMC-1 has a slot of a 3×3 array of square patches while 7×7 array of AMC-2 has a slot due to removal of central square patch. (iii) At $h = 3.0$ mm and $h' = 2.5$ mm, 9×9 array AMC-1 has a slot of a 3×3 array of square patches, while 7×7 array of AMC-2 has a slot due to the removal of the central square patch. The SSMSA dimensions are optimized in each case. Impedance variation and return loss of optimized MPSSMSA with two slotted AMCs at different 'h' are shown in Fig. 12. The radiation patterns at 3.45 GHz are shown in Fig. 13. $S_{11} < -10$ dB is obtained over 3.3–3.6 GHz, and CPL < -15.4 dB, -15.9 dB, and -16.4 dB are obtained for $h = 4.0$ mm, 3.5 mm, and 3.0 mm, respectively. The CPL decreases with the decrease in substrate height. Front-to-back lobe ratio (FBR) also improves with the decrease in substrate height.

3.3. MPSSMSA in a Ring with a PP in Slotted AMC-1 and Slotted AMC-2 Surfaces

To increase the inductive impedance of MPSSMSA with two slotted AMC surfaces, a rectangular parasitic patch (PP) is fabricated in a 3×3 slot of SAMC-1on FR4 superstrate, and 7 mm square patches with the periodicity of 9 mm are fabricated around it to form a metamaterial-inspired parasitic patch (MI-PP) and placed above the MPSSMSA. It increases the inductive impedance of the antenna, which is compensated for by decreasing the substrate height. A metallic rectangular ring is also placed around the MPSSMSA to increase the inductive impedance. To compensate for it, the substrate height 'h' is decreased to 1.8 mm, and the spacing between the superstrate and SSMSA (h') is decreased to 2.4 mm. The resultant geometry is the proposed antenna. The side view of the proposed antenna with the top view of different layers is shown in Fig. 1.

The conducting metallic ring and the spacing between the ring and SSMSA are equivalent to an inductor and capacitor, respectively. The rectangular ring electromagnetically couples with SSMSA and enhances the BW of the antenna. The effect of the width of the rectangular ring '$W = (L1 - L2)/2$' and the spacing between the ring and SSMSA '$S = (L2 - L3)/2$', keeping all other parameters fixed, is analysed. The impedance variation and S_{11} for different widths of rectangular ring and spacing are shown in Fig. 14 and Fig. 15, respectively. As the width of the rectangular ring 'W' increases, the inductive impedance increases due to the increase in conducting area, and the impedance variation plot shifts upward. The resonant frequency also decreases with the increase in 'W'. As the spacing 'S' between the ring and SSMSA increases, the capacitive impedance decreases, and the impedance variation plot shifts upward. The resonant frequency decreases with the increase in 'S'. $S_{11} < -10$ dB is obtained over 3.27–3.67 GHz for $W = 28$ mm and $S = 5.8$ mm.

The impedance variation plot has a loop, which is due to electromagnetic coupling between the ring and SSMSA. The electromagnetic coupling depends on the spacing between SSMSA and the ring, and also on the dimensions of SSMSA and the ring.

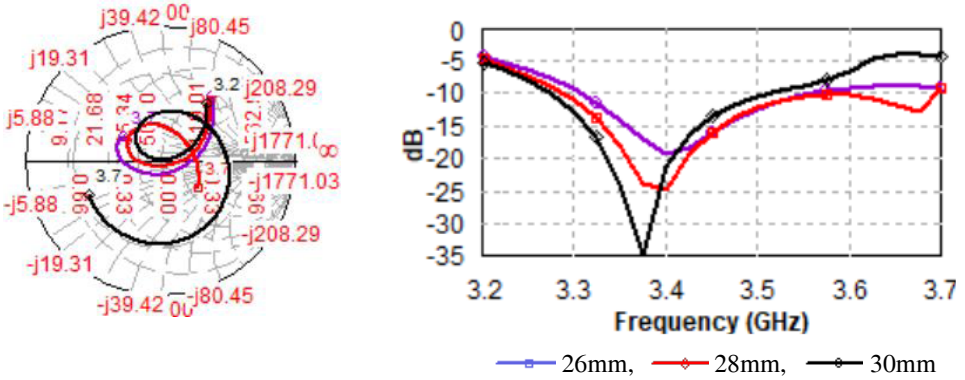

FIGURE 14. Impedance variation and return loss for different width of Ring 'W'.

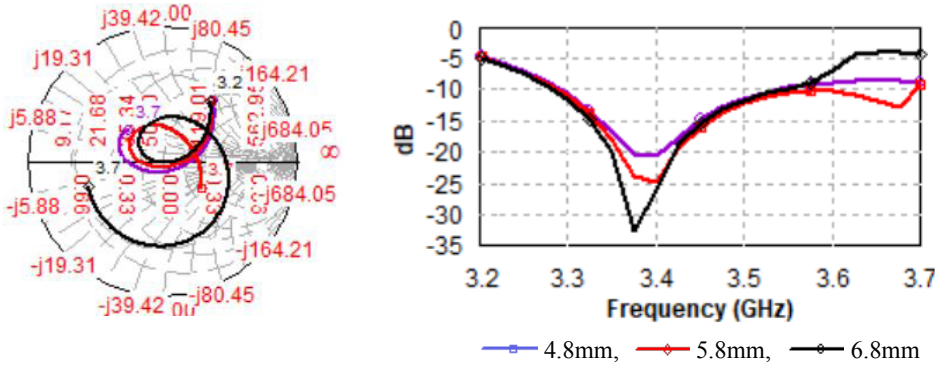

FIGURE 15. Impedance variation and return loss for different spacing 'S' between Ring and SSMSA $S = (L2 - L3)/2$.

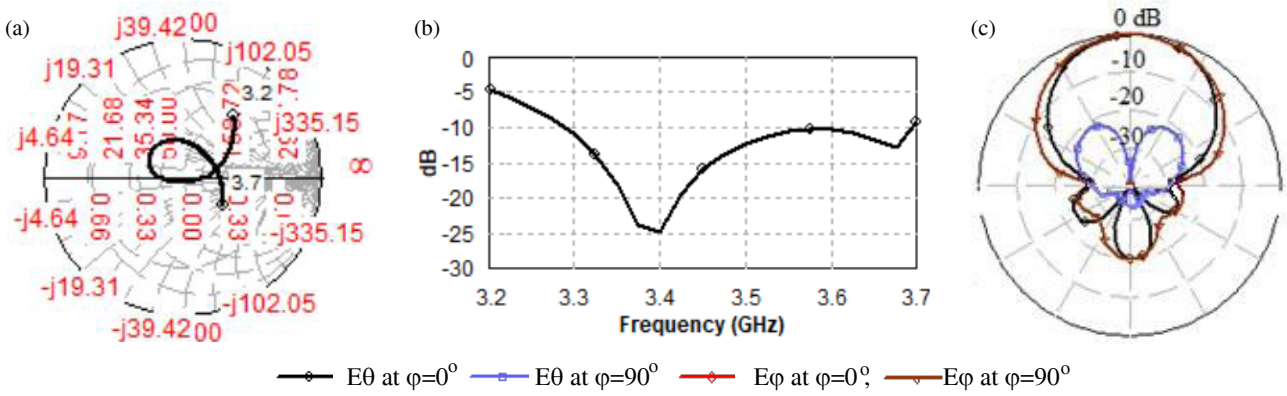

FIGURE 16. (a) Impedance variation. (b) Return loss. (c) Radiation pattern at 3.45 GHz of proposed antenna.

The rectangular ring and PP increase the inductive impedance of the antenna, which is compensated by decreasing the substrate height. The PP and the metamaterial square patch array around the PP also electromagnetically couple with the SSMSA and the ring. In MI-PP, the spacing between the patches is varied to tune and achieve the desired BW. As the spacing between square patches and PP is decreased, it intercepts more radiating near fields of SSMSA, and therefore, inductive impedance increases. It affects the impedance matching and the BW of the antenna. The dimensions of the ring, spacing between the ring and SSMSA, and dimensions of SSMSA and PP are optimized. The impedance variation and return loss of the proposed antenna are shown in Fig. 16.

The radiation pattern of the antenna at 3.45 GHz is shown in Fig. 12(c). The antenna offers < -22 dB SLL and CPL. The gain and antenna efficiency are shown in Fig. 17. The antenna offers the peak gain of 9.8 dBi, and the gain variation is < 0.5 dB over 3.3–3.6 GHz frequency band for 5G application. The gain decreases sharply after 3.65 GHz, the second resonant frequency. The $0.979\lambda_0 \times 1.03\lambda_0 \times 0.064\lambda_0$ structure has $> 80\%$ antenna efficiency, which considers conduction, dielectric, and reflection losses. The low-profile, compact, and low-cost antenna is easy to fabricate and feed. The stable radiation pattern, characterized by low SLL and CPL, makes it a suitable candidate for 5G applications.

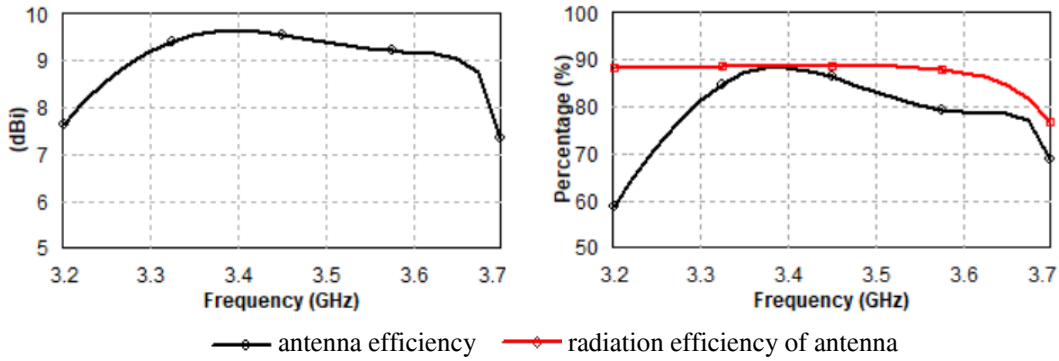

FIGURE 17. Gain and antenna efficiency, and radiation efficiency of antenna.

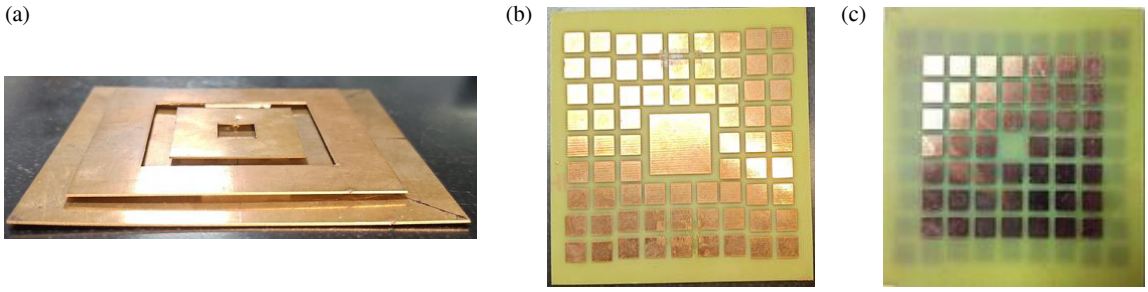

FIGURE 18. Different layers of the fabricated antenna. (a) Metal-plated SSMSA in a ring. (b) MI-MSA. (c) Slotted AMC.

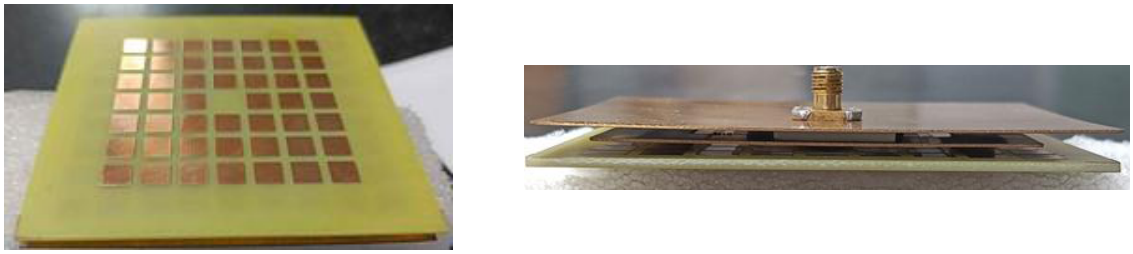

FIGURE 19. 3-dimensional views of the fabricated antenna.

4. FABRICATION AND MEASUREMENT RESULTS

The antenna structure is fabricated. A 0.5 mm-thick copper metal plate ground plane, slotted MSA, and rectangular ring are precisely cut using Auto CAD and LASER technology. The PP with a nonuniform metasurface and slotted AMC are fabricated using photo-lithography technique on an FR4 superstrate. The metal-plated SSMSA in a ring, top view of MI-PP, and slotted AMC layer are shown in Fig. 18, while 3-dimensional views of the antenna are shown in Fig. 19.

S_{11} is measured using an Agilent N9916A network analyzer. Simulated and measured S_{11} are shown in Fig. 20. The measured minimum S_{11} is -21.6 dB, while the simulated minimum S_{11} is -23.8 dB at 3.4 GHz. The radiation patterns are measured using a standard horn antenna and an Agilent N 9916A network and spectrum analyzer in an anechoic chamber. The standard horn antenna is connected to the Agilent network analyzer N 9916A, and the proposed antenna is connected to the Agilent Spectrum analyzer. The distance between the two antennas is kept more than $2D^2/\lambda$ to ensure measurement in the far-field region; D is the maximum dimension of the antenna, and λ is the wavelength corresponding to the operating frequency. The transmitting (Tx) antenna and receiving (Rx) antenna are aligned and face each other in the E-plane. Both antennas are rotated by 90° to measure the radiation pattern in the H-plane. The Tx antenna in the E-plane and Rx antenna in the H-plane, or vice versa, provide cross-polar radiation. In all

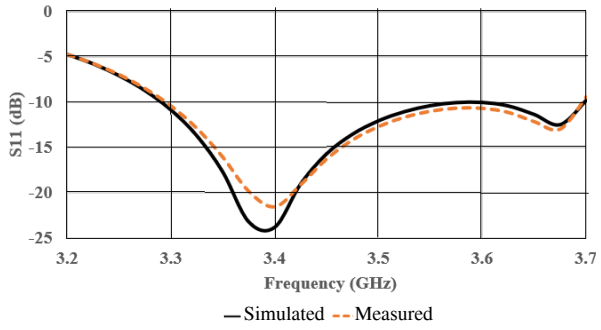

FIGURE 20. Simulated and measured S_{11}.

TABLE 1. Comparison of the proposed antenna with reported state-of-the-art antennas.

Ref.	*Polar-ization*	*Gain (dBi)*	BW(GHz)/ *BW (%)*	*SLL (dB)*	*CPL (dB)*	*FBR (dB)*	*Size* ($\lambda_0 \times \lambda_0 \times \lambda_0$)
[9]	CP	5.9	8.6–11.2/37.2	−12	−8	12	$0.62 \times 0.62 \times 0.064$
[12]	CP	5.5	2.0–4.4/75	−10	−13	16	$0.45 \times 0.45 \times 0.007$
[13]	LP	12.1	3.52–6.44/58.6	−18	−10	13	$1.66 \times 1.66 \times 0.05$
[15]	LP	12.5	5.14–6.56/24.3	−20	−15	20	$1.55 \times 1.55 \times 0.11$
[16]	LP	12.3	5.0–6.4/24.6	−19	−18	20	$1.52 \times 1.52 \times 0.1$
[18]	LP	7.8	2.38–3.18/28	−17	−15	15	$0.53 \times 0.53 \times 0.035$
[19]	LP	8.3	3.3–3.6/8.7	−20	−20	20	$0.94 \times 0.99 \times 0.046$
This work	LP	9.8	3.3–3.65/10.1	−22	−22	20	$0.98 \times 1.03 \times 0.064$

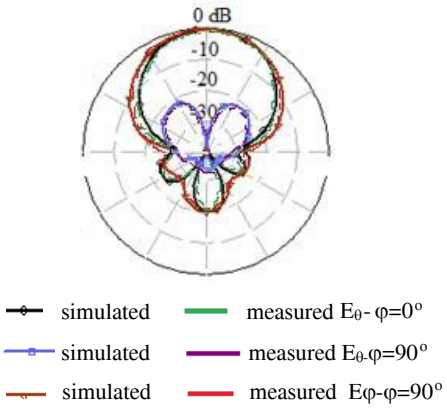

FIGURE 21. Simulated and measured radiation patterns at 3.45 GHz.

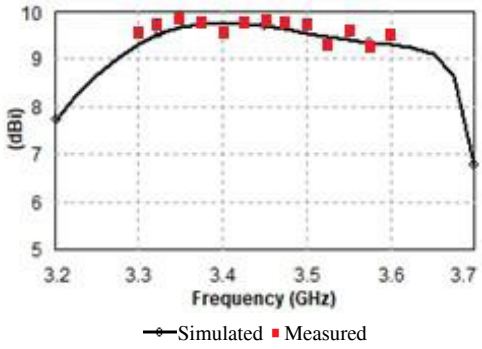

FIGURE 22. Simulated and measured gains.

four cases, the Tx antenna is kept fixed, while the Rx antenna is rotated from 0° to 360°. Antenna gain is calculated using the Friis transmission equation, considering cable, connector, and adapter losses. The simulated and measured gain variations and radiation patterns at 3.45 GHz are shown in Figs. 21 and 22, respectively. The Simulated CPL is < -22 dB, while the measured CPL is < -22.9 dB. The simulated antenna gain varies from 9.3 to 9.8 dBi, while the measured antenna gain varies from 9.14 to 9.94 dBi. The measured results closely follow the simulated ones. The discrepancy in measured and simulated results may be attributed to fabrication errors, connector loading, nonuniform dielectric constant of the superstrate, and misalignment of different layers.

5. COMPARISON WITH STATE-OF-THE-ART ANTENNAS

The proposed antenna is compared with low-profile metamaterial-based state-of-the-art antennas in terms of bandwidth, peak gain, SLL, CPL, and FBR in Table 1. Both Linearly Polarized (LP) and CP antennas are considered. The antennas in [9, 12, 18] have smaller dimensions than the proposed antenna, but these antennas offer less gain and higher SLL, CPL, and FBR. Antennas in [13–15] have larger gain but also have larger dimensions and higher SLL, CPL, and FBR than the proposed antenna. The structure in [19] is comparable in size and offers SLL and CPL less than −20 dB, but the proposed antenna offers higher gain and better SLL, CPL, and FBR.

6. CONCLUSION

A stacked metal-plated slotted MSA in a ring using multiple metasurfaces is designed to offer high gain and stable radiation patterns for 5G applications. The slot and nonuniform spacing between patches of the metasurface help in optimizing the structure to operate over the desired band. The metasurface around PP and slotted AMC increases the inductive impedance of the structure; therefore, MSA height from the ground plane is reduced to enhance the capacitive impedance. It results in the decrease in CPL due to radiation from the probe feed. The low-cost, simple to design and fabricate structure offers the peak gain of 9.8 dBi, antenna efficiency $> 80\%$, SLL and CPL < -22 dB, and the gain variation < 0.5 dB over 3.3–3.6 GHz frequency band.

REFERENCES

[1] Kumar, G. and K. P. Ray, *Broadband Microstrip Antennas*, Artech House, 2003.

[2] Chopra, R. and G. Kumar, "Broadband and high gain multilayer multiresonator elliptical microstrip antenna," *IET Microwaves, Antennas & Propagation*, Vol. 14, No. 8, 821–829, 2020.

[3] Raha, K. and K. P. Ray, "Broadband high gain and low cross-polarization double cavity-backed stacked microstrip antenna," *IEEE Transactions on Antennas and Propagation*, Vol. 70, No. 7, 5902–5906, 2022.

[4] Sivanagaraju, N. and M. S. S. Ram, "Design and analysis of wideband circularly polarized antenna loaded with ring structure," *Progress In Electromagnetics Research C*, Vol. 158, 57–61, 2025.

[5] Chopra, R. and G. Kumar, "High gain broadband stacked triangular microstrip antennas," *Microwave and Optical Technology Letters*, Vol. 62, No. 9, 2881–2888, 2020.

[6] Liu, S., W. Wu, and D.-G. Fang, "Single-feed dual-layer dual-band E-shaped and U-slot patch antenna for wireless communication application," *IEEE Antennas and Wireless Propagation Letters*, Vol. 15, 468–471, 2016.

[7] Kumar, P., T. Ali, and M. M. M. Pai, "Electromagnetic metamaterials: A new paradigm of antenna design," *IEEE Access*, Vol. 9, 18 722–18 751, 2021.

[8] Milias, C., R. B. Andersen, P. I. Lazaridis, Z. D. Zaharis, B. Muhammad, J. T. B. Kristensen, A. Mihovska, and D. D. S. Hermansen, "Metamaterial-inspired antennas: A review of the state of the art and future design challenges," *IEEE Access*, Vol. 9, 89 846–89 865, 2021.

[9] Zheng, Q., C. Guo, J. Ding, and G. A. E. Vandenbosch, "Use of non-uniform RIS and parasitic strips to improve antenna CP performance," *IET Microwaves, Antennas & Propagation*, Vol. 14, No. 14, 1795–1802, 2020.

[10] Srivastava, K., S. Kumar, S. Dwari, B. K. Kanaujia, H. C. Choi, and K. W. Kim, "Anisotropic meta-surface-based wideband high gain circularly polarized patch antenna," *Electromagnetics*, Vol. 40, No. 8, 594–604, 2020.

[11] Guthi, S. and V. Damera, "High gain and wideband circularly polarized S-shaped patch antenna with reactive impedance surface and frequency-selective surface configuration for Wi-Fi and Wi-Max applications," *International Journal of RF and Microwave Computer-Aided Engineering*, Vol. 31, No. 11, e22865, 2021.

[12] Ni, C., L. Zhang, and Z. Zhang, "A low profile broadband circularly polarized metasurface antenna based on tri-modal," *IEEE Antennas and Wireless Propagation Letters*, Vol. 23, No. 10, 3267–3271, 2024.

[13] De Dieu Ntawangaheza, J., L. Sun, C. Yang, Y. Pang, and G. Rushingabigwi, "Thin-profile wideband and high-gain microstrip patch antenna on a modified AMC," *IEEE Antennas and Wireless Propagation Letters*, Vol. 18, No. 12, 2518–2522, 2019.

[14] Singh, A. K., M. P. Abegaonkar, and S. K. Koul, "Compact near zero index metasurface lens with high aperture efficiency for antenna radiation characteristic enhancement," *IET Microwaves, Antennas & Propagation*, Vol. 13, No. 8, 1248–1254, 2019.

[15] Jagtap, S., A. Chaudhari, N. Chaskar, S. Kharche, and R. K. Gupta, "A wideband microstrip array design using RIS and PRS layers," *IEEE Antennas and Wireless Propagation Letters*, Vol. 17, No. 3, 509–512, 2018.

[16] Rochkari, A., S. Verulkar, M. Trimukhe, V. Bodade, and R. Gupta, "Low profile high gain wideband stacked MSA array for 5G, WLAN and C-band applications," *International Journal of Microwave & Optical Technology*, Vol. 19, No. 1, 80, 2024.

[17] Singh, A. K., M. P. Abegaonkar, and S. K. Koul, "Miniaturized multiband microstrip patch antenna using metamaterial loading for wireless application," *Progress In Electromagnetics Research C*, Vol. 83, 71–82, 2018.

[18] Meng, F., Y. Liu, and S. K. Sharma, "A miniaturized patch antenna with enhanced bandwidth by using reactive impedance surface ground and coplanar parasitic patches," *International Journal of RF and Microwave Computer-Aided Engineering*, Vol. 30, No. 7, e22225, 2020.

[19] Rochkari, A., S. Verulkar, N. Chaskar, M. Trimukhe, and R. Gupta, "Cross polar reduction of a high gain wide-band stacked microstrip antenna using metasurfaces," *Progress In Electromagnetics Research Letters*, Vol. 119, 91–98, 2024.

[20] Singh, A. K., M. P. Abegaonkar, and S. K. Koul, *Metamaterials for Antenna Applications*, CRC Press, 2021.

[21] Tadesse, A. D., O. P. Acharya, and S. Sahu, "Application of metamaterials for performance enhancement of planar antennas: A review," *International Journal of RF and Microwave Computer-Aided Engineering*, Vol. 30, No. 5, e22154, 2020.

[22] Paul, S. and M. J. Akhtar, "Near field microwave subsurface imaging using metasurface loaded planar antenna and synthetic aperture radar (SAR) technique," *International Journal of RF and Microwave Computer-Aided Engineering*, Vol. 31, No. 10, e22800, 2021.

[23] Ni, C., Z. Yu, L. Zhang, and Z. Zhang, "A wideband circularly polarized and beam deflection antenna based on two metasurfaces," *IEEE Antennas and Wireless Propagation Letters*, Vol. 22, No. 12, 2861–2865, 2023.

[24] Ni, C., M. S. Chen, Z. X. Zhang, and X. L. Wu, "Design of frequency-and polarization-reconfigurable antenna based on the polarization conversion metasurface," *IEEE Antennas and Wireless Propagation Letters*, Vol. 17, No. 1, 78–81, 2018.

[25] Ji, L.-Y., P.-Y. Qin, and Y. J. Guo, "Wideband Fabry-Perot cavity antenna with a shaped ground plane," *IEEE Access*, Vol. 6, 2291–2297, 2017.

[26] Chaskar, N., S. Jagtap, R. Thakare, and R. Gupta, "Gain flattening of wideband FPC antenna using elliptical and rectangular slotted AMC layers," *Progress In Electromagnetics Research C*, Vol. 110, 81–89, 2021.

[27] Rochkari, A., V. Yadav, M. Trimukhe, N. Chaskar, M. Awasthi, and R. Gupta, "Meta-surfaces based high gain wide-band stacked antenna with low cross-polarization and side lobe level for 5G applications," *Progress In Electromagnetics Research C*, Vol. 153, 179–188, 2025.